Supporting Information

Designing Different Carbon Capping Amorphous MoO_2 to Enhance Electrochemical Performance in Lithium-Ion Batteries

Gaoyuan Liu[a], Xinxin Yin[a], Jing Xie[a], Jindou Hu[a], Aize Hao[b], Zhenjiang Lu[a, *] and Yali Cao[a, *]

[a] State Key Laboratory of Chemistry and Utilization of Carbon Based Energy Resources, College of Chemistry, Xinjiang University, Urumqi 830017, Xinjiang, PR China.

[b] School of Chemical Engineering, Sichuan University of Science and Engineering, Zigong 643000, China

*Corresponding author.

E-mails: caoyali523@163.com (Yali Cao); luzj@xju.edu.cn (Zhenjiang Lu).

Experimental Section

1.1 Materials characterization

The morphologies of samples were obtained on a Hitachi S-4800 scanning electron microscope with an accelerating voltage of 15 kV, and high-resolution transmission electron microscopes (HRTEM) with an accelerating voltage of 200 kV (JEOL JEM-2010F electron microscope). The element component of MoO_{2-x}@C was measured by the energy disperse X-ray spectrum (EDS, EDAXTLS). To acquire the crystal structure of samples, X-ray powder diffraction (XRD) was obtained by Bruker D8 employing Cu-Kα radiation (1.54056 Å) with an operating voltage of 40 kV and a beam current of 40 mA. The electron paramagnetic resonance (EPR) data was tested by the Bruker A300. The g-values for each EPR spectrum were extracted from simulations performed using EasySpin (v5.2.23). The Raman spectra was collected by employing Raman spectroscopy (Bruker Senterra) with excitation light source of 532 nm. The surface components and valence states of samples were characterized by X-ray photoelectron spectra (XPS) (Thermo Fisher Scientific ESCALAB250Xi) employing Al Kα (1486.6 eV). Thermal stability of the samples was assessed by thermal gravimetric (TGA, NETZSC-ATA449C) analysis in air at a heating rate of 10°C min^{-1}. The specific surface area, pore size and pore volume of the samples were obtained by Brunauer-Emmett-Teller (BET) methods through N_2 adsorption-desorption isotherms (Quantachrome, Autosorb-iQ2). Before testing, all samples were degassed at 300°C for 9 h to remove the moisture and physical adsorbed gases.

1.2 Electrochemical characterization

The anode was fabricated by mixing MoO_{2-x}@C (70 wt%), acetylene black (20 wt%), and polyvinylidene fluoride (10 wt%) dissolved in N-methyl-2-pyrrolidinone, and then coated on the Cu foil and were finally dried in a vacuum oven at 110°C for 12 h. The average mass loading of the whole electrode is≈0.6-1.0 mg cm^{-2}. The CR2025 type cells were assembled in a glove box under Ar atmosphere (< 0.01 ppm of oxygen and water). For lithium-ion batteries (LIBs), it consisted of a prepared electrode, glass

fibers separator (Celgard 2500), and lithium foil as the counter electrode. The electrolyte was 1 M $LiPF_6$ in ethylene carbonate (EC)/dimethyl carbonate (DMC)/diethyl carbonate (DEC) (1:1:1 by volume) with 5 vol.% fluoroethylene carbonate (FEC) additive as the electrolyte.

A full cell was assembled using the preactivated MoO_{2-x}@C anode and lithium cobalt oxide (LCO) cathode with an active materials weight ratio of 1:3 for MoO_{2-x}@C-450||LCO. The cathode was prepared by mixing LCO (70 wt%), acetylene black (20 wt%), and polyvinylidene fluoride (10 wt%) dissolved in N-methyl-2-pyrrolidinone, and then coated on the aluminum foil, which were finally dried in a vacuum oven at 110°C for 12 h.

Cyclic voltammetry (CV) was conducted on a CHI760E workstation (CHI760E, Chenhua, China) within the potential range of 0.01–3 V. Electrochemical impedance spectroscopy (EIS) was carried out by using electrochemical workstation (CHI760E, Chenhua, China) within the frequency range of 100 kHz to 0.01 Hz under open circuit voltage. The galvanostatic charge/discharge measurements were carried out with a battery testing system (Land CT2001A, Wuhan, China) in the voltage range of 0.01–3.0 V at room temperature.

1.3 Calculation of the full battery capacity energy and power densities

The capacity of our full battery is calculated based on the mass of lithium cobalt oxide ($LiCoO_2$) cathode active material. The theoretical capacity of the material is calculated as follows:

$$LiCoO_2 = xLi^+ + Li_{(1-x)}CoO_2$$

$$C = nF/3.8M \qquad (1)$$

In this formula n is the number of electrons participating in the reaction F is Faraday's constant M is the molar mass of $LiCoO_2$. 1 mol of electrons is 96485C,

assuming that the material occurs n electron reaction that 1 mol of active material electrochemical reaction generated by the amount of electricity is 96485n C. 1 g electrode material theoretically discharged electricity: 1 mAh = 1×10^{-3} A×3600 s = 3.6 C, the full battery in the mass of $LiCoO_2$ is 2 mg, then theoretically discharged electricity 2×3.6 C = 7.2 C. Assuming that Li in $LiCoO_2$ can be completely removed then the number of transferred electrons n is 1 and according to the above formula 1, the specific process can be calculated as 96485×1/(7.2×98) = 136.7 mAh g^{-1}. However, the actual capacity of the full-battery discharged for the first time is 121.3 mAh $g^{-}1$, so the number of electrons involved in the reaction is n=(121.3×7.2×98)/96485=0.9. From the fact that the number of electrons participating in the reaction is 0.9, it can be deduced that there are 0.9 mol of Li^+ embedded in $LiCoO_2$ in the first discharge.

In full cell tests, the calculations of energy (E, Wh kg^{-1}) and power densities (P, W kg^{-1}) based on the total mass of both anode and cathode materials were performed.

$$P = \Delta V \times i/m \qquad (2)$$

$$E = P \times t/3600 \qquad (3)$$

$$\Delta V = V_{max} - V_{min} \qquad (4)$$

In which t (s) is the discharge time, i (A) is the charge/discharge current, m (Kg) is the total mass of active materials in both anode and cathode, V_{max} (V) is the discharge potential excluding the IR drop and V_{min} (V) is the potential at the end of discharge voltages. where i (A) is 54.64 μA, m is 2 mg, Vmax is 4.0833 V, Vmin is 1 V, and the energy density E is 421.0 Wh kg^{-1} according to Equation 2-4.

Results and discuss

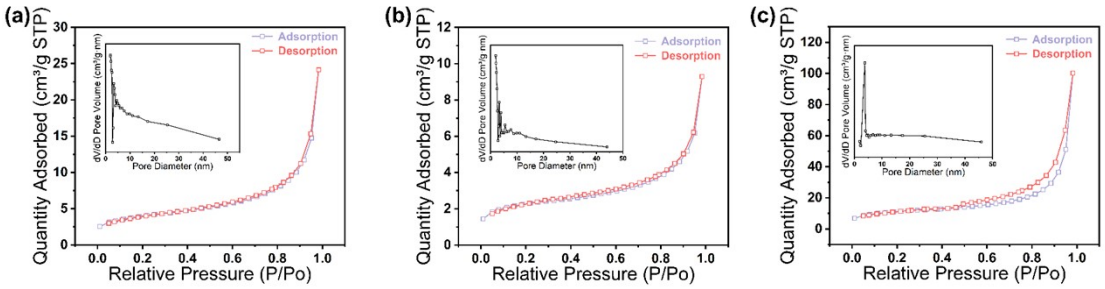

Fig. S1 Pore size distribution of (a) MoO_{2-x}@C-450, (b) MoO_{2-x}@C-CNF-450 and (c) MoO_{2-x}@C-PDA-450.

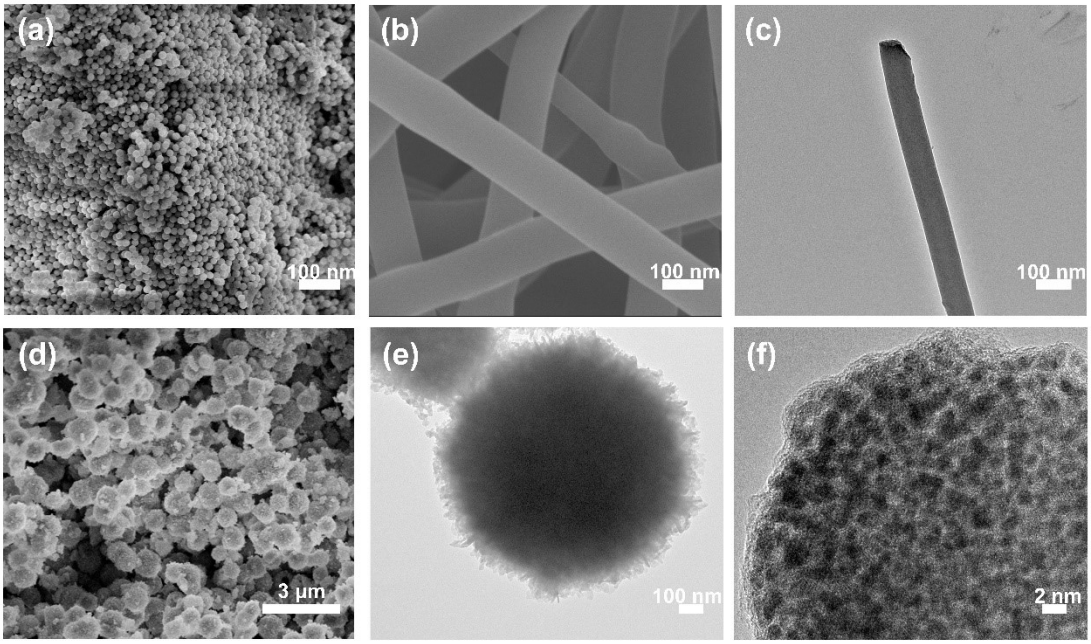

Fig. S2 Wide-angle SEM image of (a) Mo-MI precursor. (b) SEM images of MoO_{2-x}@C-CNF. (c) TEM images of MoO_{2-x}@C-CNF. (d) SEM images of MoO_{2-x}@C-PDA. (e) TEM images of MoO_{2-x}@C-PDA (f) the HRSEM image of MoO_2@C

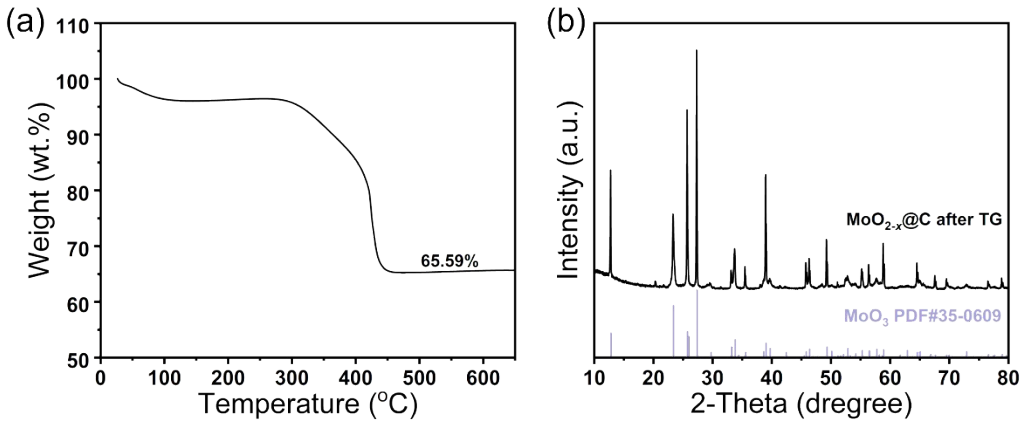

Fig. S3 (a) TGA curve of prepared MoO_{2-x}@C-450 in air. (b) XRD pattern of the sample after TGA text of MoO_{2-x}@C-450.

In terms of the TGA curve, the residual weight of the sample after heating to 600 °C is approximately 65.59 wt.%, which can be attributed to MoO3. Therefore, the carbon content can be calculated using the following equation:

m (carbon) = 1 – 65.59 ωt.%*M(MoO_2)/M(MoO_3) = 1 – 65.59 ωt.%*128/144 ≈ 41.69ωt.%

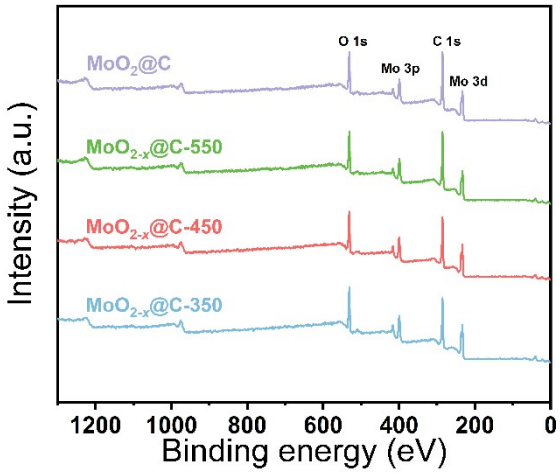

Fig. S4 XPS spectra of MoO_2@C and MoO_{2-x}@C-350/450/550.

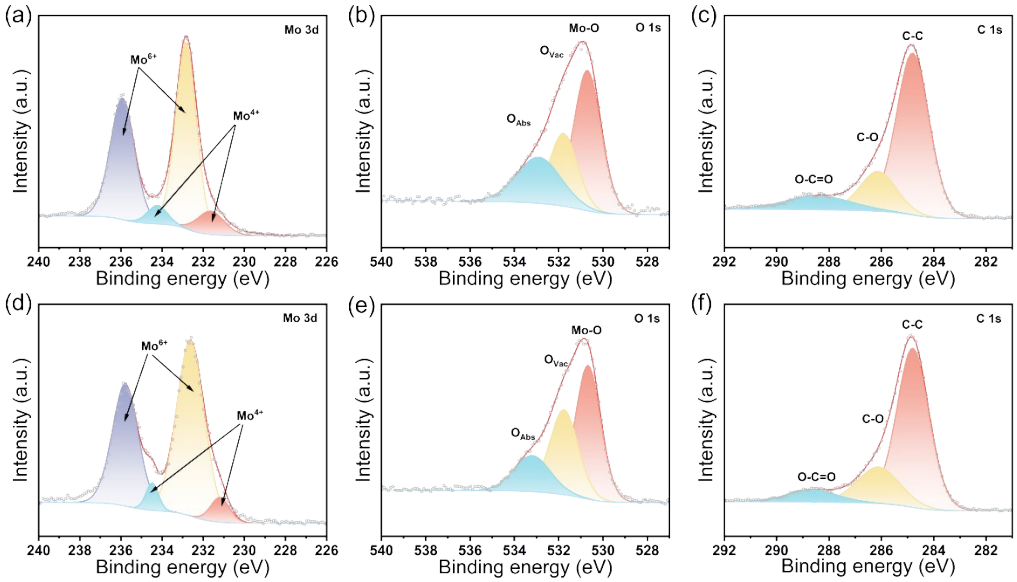

Fig. S5 XPS spectra of (a)Mo 3d, (b) O 1s, (c) C 1s (MoO_{2-x}@C-350), (d) Mo 3d, (e) O 1s, (f) C 1s (MoO_{2-x}@C-550).

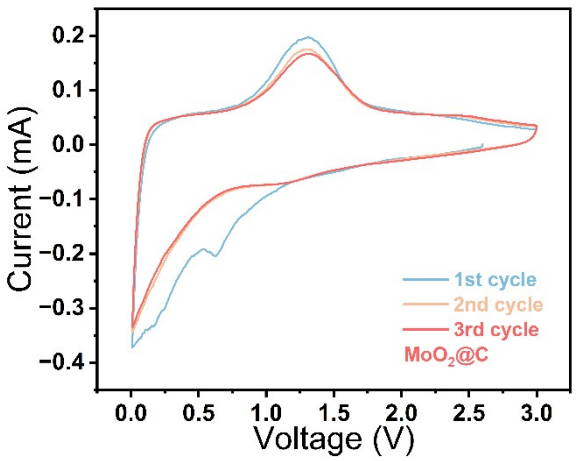

Fig S6 Cyclic voltammetry profiles of MoO_2@C.

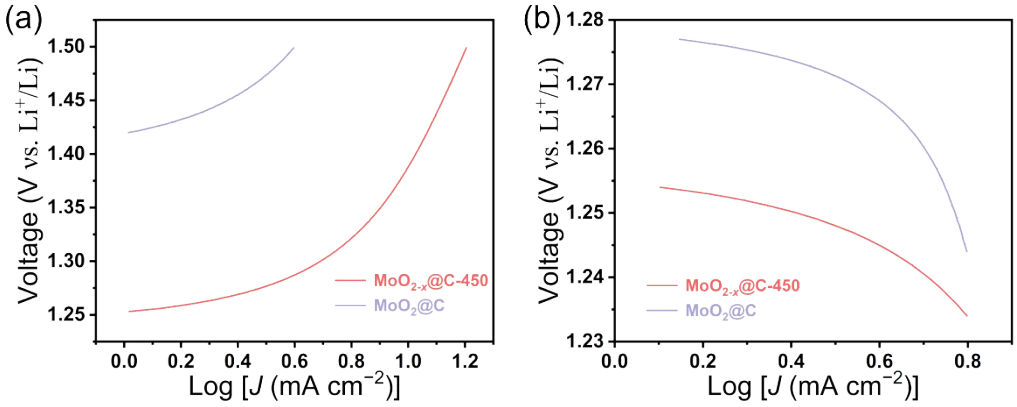

Fig. S7 Tafel plots of (a) oxidation and (b) reduction processes for MoO_{2-x}@C-450 and MoO_2@C.

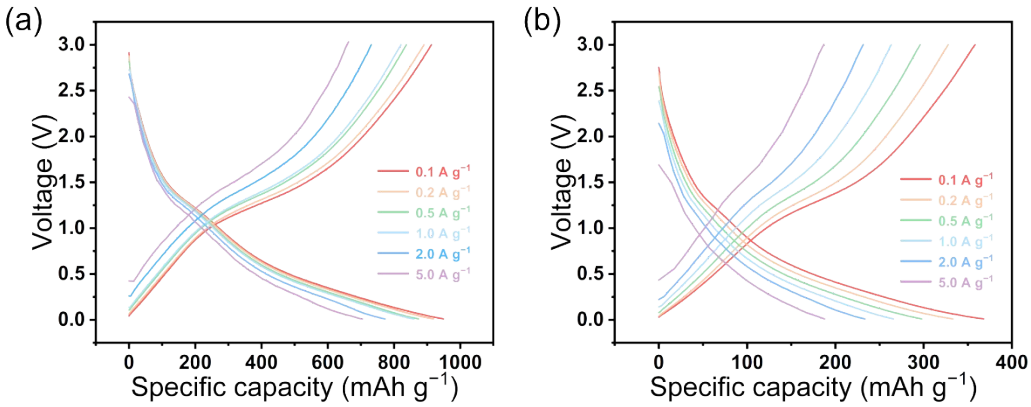

Fig. S8 Selected discharge-charge profiles of (a) MoO_{2-x}@C and (b) MoO_2

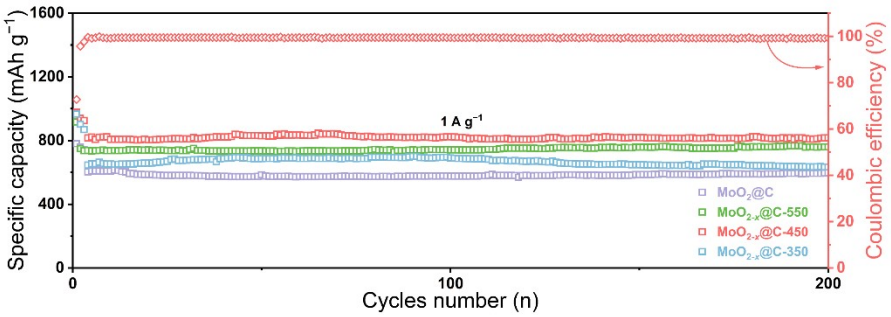

Fig. S9 The cycling performance of MoO_{2-x}@C-350/450/550 and MoO_2@C.

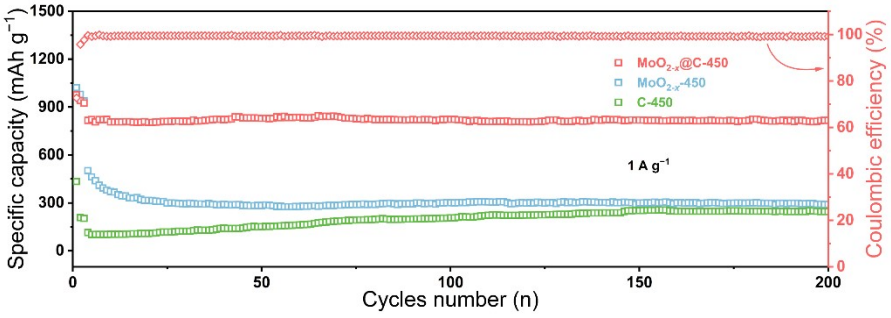

Fig. S10 The cycling performance of MoO_{2-x}@C-450, MoO_{2-x}-450 and C-450.

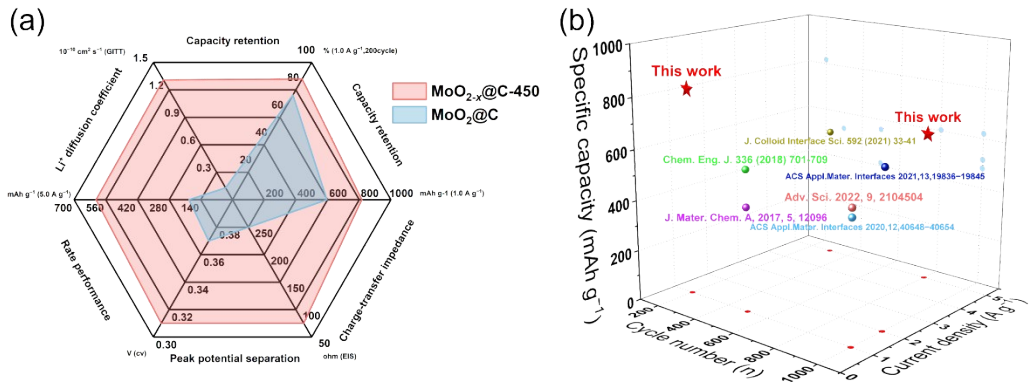

Fig. S11 (a) Comparative properties of MoO_{2-x}@C-450 and MoO_2@C. (b) Comparative specific capacity of MoO_2@C and the modified materials in other references.

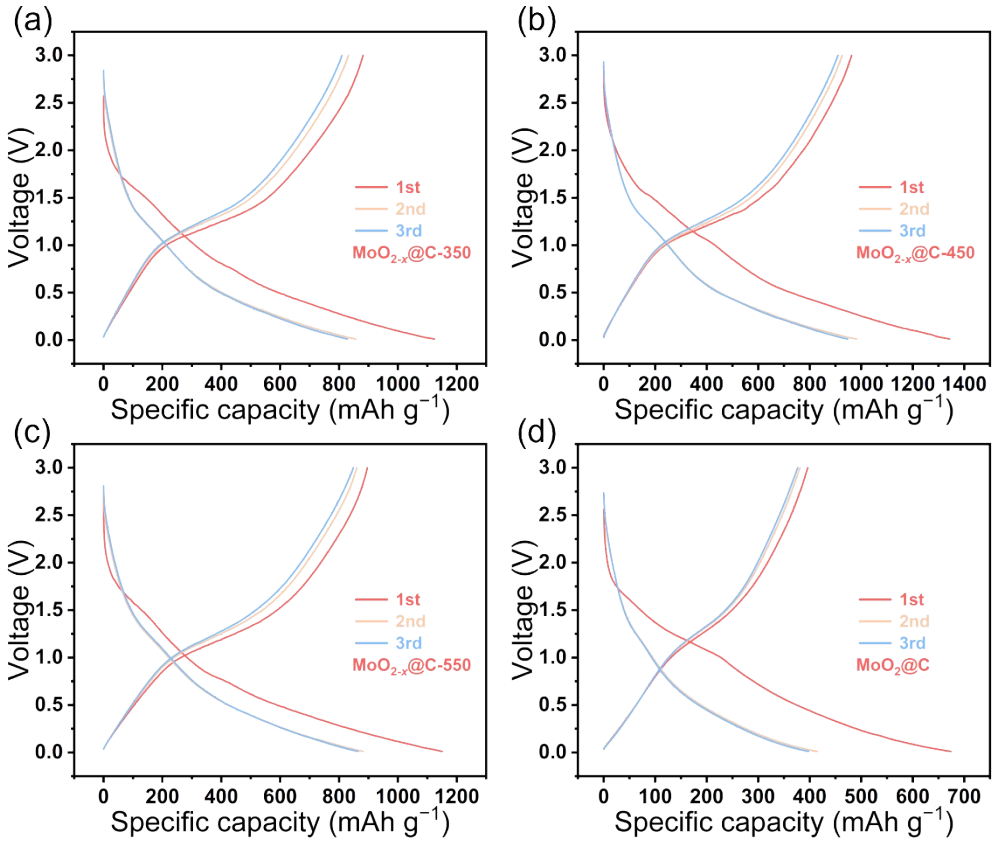

Fig. S12 Partial discharge-charge curves for (a) MoO_{2-x}@C-350, (b) MoO_{2-x}@C-450, (c) MoO_{2-x}@C-550 and (d) MoO_2@C.

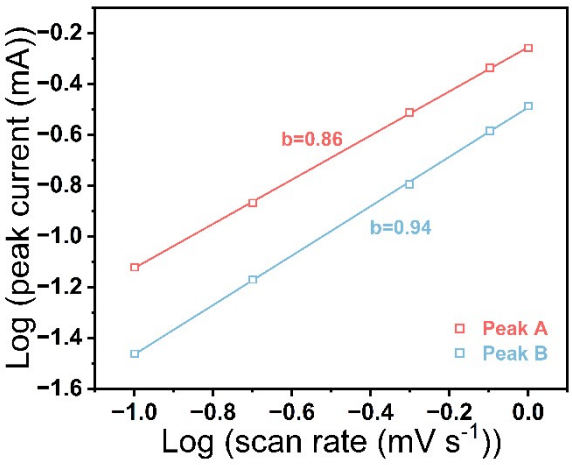

Fig. S13 The b-values calculated from CV curves.

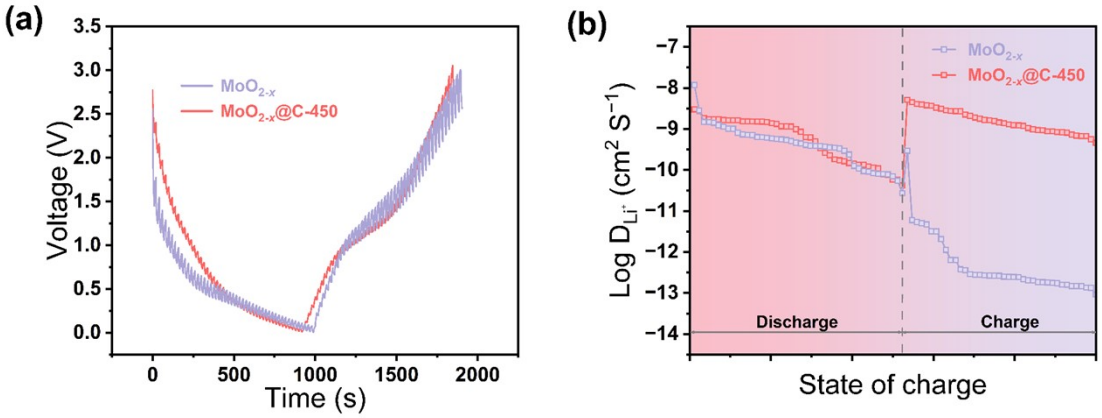

Fig. S14 (a) GITT curves for MoO_{2-x}@C-450and MoO_{2-x}. (b) The log(D_{Li^+}) values in discharge state and charge states for MoO_{2-x}@C-450 and MoO_{2-x}.

Table S1. Comparison of electrochemical performance of MoO_2-based anodes.

Electrode Materials	Current Rate ($A\ g^{-1}$)	Remaining Capacity ($mAh\ g^{-1}$) /Number of Cycle (n)	Ref.
MoO_{2-x}@C	5.0	601.4(800)	This work
MoO_2 nanotextiles	0.3	860.4(160)	[1]
MoO_2/N-C	0.1	708.0(100)	[2]
MoO_2/C	1.0	480.0(1000)	[3]
MoO_2@C	1.0	669.1(1000)	[4]
MoO_2/N-doped carbon	5.0	531.0(300)	[5]
MoO_2/NPC@rGO	10.0	249.5(1000)	[6]
MoO_2@MoS_2	0.5	650.0(500)	[7]
Meso-MoO_2/MoP-NBs	1.0	515.0(1000)	[8]
MoO_2-Mo_2C-C	0.1	1188.0(250)	[9]
Sb/MoO_2@CNFs	1.0	558.0(500)	[10]
MoO_2/Sn/NC@NC	2.0	620.1(1000)	[11]
$Li_4Ti_5O_{12}$-TiO_2/MoO_2	1.0	413.0(500)	[12]
Mo_2C-MXene@MoO_2@C	0.5	854.5(500)	[13]

Table S2. Comparison of electrochemical performance of Mo-based anodes.

Electrode Materials	Current Rate ($A\ g^{-1}$)	Remaining Capacity ($mAh\ g^{-1}$) /Number of Cycle (n)	Ref.
MoO_{2-x}@C	5.0	601.4(800)	This work
Ni/Mo_2C/NC	2.0	412.7(1800)	[14]
MoS_2-Mo_2C@C	2.0	598.1	[15]
MoS_2/Graphite	1.0C	58.3(300)	[16]
Mo_3Se_4@$Ti_3C_2T_x$	1.5C (1C equals to 670 $A\ g^{-1}$)	790.8	[17]
Mo_2CT_x/Mo_2C	1.0	340.0(1000)	[18]
β-Mo_2C	2.0	72.2(1500)	[19]
MON-QD/NG	5.0	297.2(300)	[20]
MoO_3/C	0.5	621.0(200)	[21]
MoO_2@Mo_2N@C	1.0	652.0(1000)	[22]
PPy@h-MoO_3	0.1	289.0(50)	[23]
MoS_2/SnS	2.0	872.7(300)	[24]
Mo_6Te_8	1.0	436.0	[25]
Ni_3Se_4/$MoSe_2$/rGO	2.0	573.3(600)	[26]
SnO_2/MoO_{3-x}/rGO	5.0	450.6(1000)	[27]
$Fe_2Mo_3O_8$/MoO_2@C	5.0	460.6(1000)	[28]
MoO_2-Li_2MoO_4	0.5	494.1(200)	[29]

Reference

1 G. Q. Xu, P. Liu, Y. R. Ren, X. B. Huang, Z. G. Peng, Y. G. Tang, H. Y. Wang, Three-dimensional MoO_2 nanotextiles assembled from elongated nanowires as advanced anode for Li ion batteries, *J. Power Sources*, 2017, **361**, 1.

2 H. H. Sun, Y. Zhang, H. Y. Liu, X. Y. Zhang, J. G. Wang, Constructing hierarchical MoO_2/N-doped carbon hydrangea-like spheres with superior lithium storage properties, *J. Alloy. Compd.*, 2019, **787**, 45.

3 Y. Yao, Z. A. Chen, R. H. Yu, Q. Chen, J. X. Zhu, X. F. Hong, L. Zhou, J. S. Wu, L. Q. Mai, Confining ultrafine MoO_2 in a carbon matrix enables hybrid Li ion and Li metal storage, *ACS Appl. Mater. Interfaces*, 2020, **12**, 40648.

4 H. Z. Xu, C. Gao, Z. Y. Cheng, L. H. Kong, W. Li, X. C. Dong, J. J. Lin, Metal oxyacid salts-confined pyrolysis towards hierarchical porous metal oxide@carbon (MO@C) composites as lithium-ion battery anodes, *Nano Res.*, 2023, **16**, 6903.

5 C. Zheng, W. X. Wu, Q. X. Deng, Y. F. Li, M. D. Wei, Nanocomposite of ultra-small MoO_2 embedded in nitrogen-doped carbon: In situ derivation from an organic molybdenum complex and its superior Li-Ion storage performance, *J. Colloid Interface Sci.*, 2021, **592**, 33.

6 J. Li, H. Wei, F. Hu, Z. Xie, J. P. Hei, Y. Q. Kong, X. J. Yin, N. N. Wang, H. H. Wei, In-situ synthesis of two-dimensional sheet-like MoO_2/NPC@rGO as advanced anode for alkali metal ion batteries, *Int. J. Hydrog. Energy*, 2022, **47**, 32594.

7 H. Sun, J. L. Xu, J. D. Huang, G. H. Li, J. Luo, M. J. Rao, Z. W. Peng, T. Jiang, Facile synthesis of hetero-structured few-layer MoS_2-coated MoO_2 as superior anode materials of lithium ion batteries, *J. Alloy. Compd.*, 2021, **851**, 156726.

8 Y. H. Shen, Y. L. Jiang, Z. Z. Yang, J. Dong, W. Yang, Q. Y. An, L. Q. Mai, Electronic structure modulation in MoO_2/MoP heterostructure to induce fast electronic/ionic diffusion kinetics for lithium storage, *Adv. Sci.*, 2022, **9**, 2104504.

9 X. Yang, Q. Li, H. J. Wang, J. Feng, M. Zhang, R. Yuan, Y. Q. Chai, In-situ carbonization for template-free synthesis of MoO_2-Mo_2C-C microspheres as high-performance lithium battery anode, *Chem. Eng. J.*, 2018, **337**, 74.

10 X. Lu, P. Wang, K. Liu, C. M. Niu, H. K. Wang, Encapsulating nanoparticulate Sb/MoO_x into porous carbon nanofibers via electrospinning for efficient lithium

storage, *Chem. Eng. J.*, 2018, **336**, 701.

11 H. J. Wang, H. Wang, D. X. Zhang, G. Chen, L. Chen, N. Zhang, R. Z. Ma, X. H. Liu, Double confined MoO_2/Sn/NC@NC nanotubes: solid–liquid synthesis, conformal transformation, and excellent lithium-ion storage, *ACS Appl. Mater. Interfaces*, 2021, **13**, 19836.

12 Y. Yang, S. T. Wang, M. C. Luo, W. Wang, F. Lv, Z. L. Tang, S. J. Guo, $Li_4Ti_5O_{12}$-TiO_2/MoO_2 nanoclusters-embedded into carbon nanosheets core/shell porous superstructures boost lithium ion storage, *J. Mater. Chem. A*, 2017, **5**, 12096.

13 G. L. Liu, F. Y. Xiao, T. Zhang, Y. Y. Gu, J. Li, D. L. Guo, M. W. Xu, N. T. Wu, A. Cao, X. M. Liu, In-situ growth of MoO_2@N doped carbon on Mo_2C-MXene for superior lithium storage, *Appl. Surf. Sci.*, 2022, **597**, 153688.

14 D. L. Guo, M. K. Yang, S. Xu, S. P. Zhu, G. L. Liu, N. T. Wu, A. Cao, H. Y. Mi, X. M. Liu, Ni activated Mo_2C by regulating the interfacial electronic structure for highly efficient lithium-ion storage, *Nanoscale*, 2022, **14**, 14575-14584.

15 L. Q. Wu, L. Feng, X. X. Mao, J. Y. Niu, W. H. Xin, D. Wang, Construction of porous MoS_2-Mo_2C@C aerogel for use as superior lithium-ion battery anode, *J. Energy Storage*, 2023, **70**, 108011.

16 B. S. Liu, F. Li, H. D. Li, S. H. Zhang, J. H. Liu, X. He, Z. J. Sun, Z. Q. Yu, Y. J. Zhang, X. Q. Huang, F. Guo, G. F. Wang, X. B. Jia, Monodisperse MoS_2/Graphite composite anode materials for advanced lithium ion batteries, *Molecules*, 2023, **28**, 2775.

17 R. S. Kamat, C. Padwal, H. D. Pham, X. j. Wang, L. D. Jadhav, D. P. Dubal, Selenium enriched over-oxidized Mo_3Se_4 decorated MXene as a high-performance Li-ion battery anode material, *J. Energy Storage*, 2023, **73**, 108916.

18 Z. Bayhan, J. K. El-Demellawi, J. Yin, Y. Khan, Y. J. Lei, E. Alhajji, Q. X. Wang, M. N. Hedhili, H. N. Alshareef, A laser-induced Mo_2CT_x MXene hybrid anode for high-performance Li-ion batteries, *Small*, 2023, **19**, 2208253.

19 R. A. Shi, N. P. Chen, B. Li, L. X. Zhang, T. T. Gao, W. H. Lian, Z. P. Wang, H. R. Cui, W. Song, Design of β-Mo_2C with an appropriate intercalation potential as an anode material toward lithium ion batteries, *Solid State Ion.*, 2024, **405**, 116438.

20 L. X. Wang, T. B. Zhao, R. P. Chen, H. Fang, Y. H. Yang, Y. Cao, L. S. Zhang, Molybdenum nitride and oxide quantum dot @ nitrogen-doped graphene nanocomposite material for rechargeable lithium ion batteries, *Batteries-Basel*, 2023, **9**, 32.

21 M. Guo, L. Y. Huang, C. K. Zhao, L. M. He, Y. Q. Wang, G. Dou, G. X. Zhang, X. M. Sun, Atomic Mo-NC-sourced robust MoO_3/C nanocomposite for high-performance Li-ion storage, *Sci. China-Mater.*, 2023, **66**, 3054-3064.

22 H. Z. Xu, C. Gao, L. H. Kong, D. Li, J. J. Lin, Constructing hierarchical porous MoO2@Mo2N@C composite via a confined pyrolysis synthetic strategy towards lithium-ion battery anodes, *Chem.-Eur. J.*, 2023, **29**, e202301565.

23 R. Nadimicherla, L. Chen, S. D. Raut, W. C. Cho, PPy@h-MoO_3 nanorods as the cathode material for high-efficiency lithium-ion batteries, *New J. Chem*, 2024, **48**, 12315-12322.

24 Y. W. Guo, K. Liu, W. L. Liu, N. Zhang, X. D. Sun, S. Li, Z. S. Wen, J. C. Sun, MoS_2/SnS heterostructure composite for high-performance lithium-ion battery anodes, *Solid State Sci.*, 2024, **156**, 107660.

25 Y. P. Leng, J. Xu, Y. J. Zhang, Z. Q. Ran, X. G. Wang, F. C. Tsai, N. Ma, Cheverl phase Mo_6Te_8 nanoparticles as new anode materials for lithium-ion batteries, *J. Energy Storage*, 2024, **80**, 110298.

26 S. Jiang, R. X. Zhang, M. J. Pang, Z. Y. Song, Z. Y. Wu, Y. L. Jiao, J. G. Zhao, Carbon-coated Ni_3Se_4/$MoSe_2$/rGO nanosheet composites for lithium-ion batteries, *ACS Appl. Nano Mater.*, 2024, **20**, 23443–23453.

27 J. H. Li, L. Wei, X. K. Cui, G. X. Han, S. Y. Hou, W. C. Shen, F. Y. Kang, R. T. Lv, L. Q. Ma, Z. H. Huang, Hydrothermal synthesis of SnO_2/MoO_{3-x}/rGO ternary nanocomposites as a high-performance anode for lithium ion batteries, *Electrochim. Acta*, 2024, **503**, 144907.

28 J. Ding, Y. D. Huang, Z. J. Liu, X. C. Wang, Y. Zhang, Y. Guo, R. Sheng, D. Z. Jia, X. C. Tang, L. Wang, $Fe_2Mo_3O_8$/MoO_2@C composites with pseudocapacitive properties and fast diffusion kinetics for the anode of lithium-ion batteries, *Chem. Eng. J.*, 2022, **431**, 133984.

29 Y. X. Jia, S. L. Jiang, X. Y. Li, Q. L. Mao, T. Bashir, L. J. Gao, Exploring lithium storage mechanism and cycling stability of MoO_2 metal oxide anode composited with Li_2MoO_4, *Inorg. Chem. Commun.*, 2024, **159**, 111827.